The Effect of Dissolved Gases on the Short-Range Attractive Force between Hydrophobic Surfaces in the Absence of Nanobubble Bridging

Mehdi Azadi[1,2], Anh V. Nguyen[1] and Gleb E. Yakubov[1,3]

[1]School of Chemical Engineering, The University of Queensland, Australia

[2]Sustainable Minerals Institute, The University of Queensland, Australia

[3]School of Biosciences, Faculty of Science, University of Nottingham, United Kingdom

Abstract

The short-range attractive forces between hydrophobic surfaces are key factors in a wide range of areas such as protein folding, lipid self-assembly, and particle-bubble interaction such as in industrial flotation. Little is certain about the effect of dissolved (well-controlled) gases on the interaction forces, in particular in those systems where the formation of surface nanobubble bridges is suppressed. Here we probe the short-range attractive force between hydrophobized silica surfaces in aqueous solutions with varying but well-controlled isotherms of gas solubility. The first contact approach force measurement method using AFM shows that decreasing gas solubility results in a decrease of the force magnitude as well as shortening of its range. The behavior was found to be consistent across all four aqueous systems and gas solubilities tested. Using numerical computations, we corroborate that attractive force can be adequately explained by a multilayer dispersion force model, which accounts for an interfacial gas enrichment (IGE), resulting in the formation of a dense gas layer (DGL) adjacent to the hydrophobic surface. We found that the DGL on the hydrophobic surface is affected only by the concentration of dissolved gases and is independent of the salt type, used to control the gas solubility which excludes the effect of electrical double-layer interactions on the hydrophobic force.

Keywords: force measurement, atomic force microscopy, hydrophobic interaction, salts

1. Introduction

Hydrophobic interactions are known to be critical in a wide range of areas, including protein folding and aggregation, a lipid assembly, particle-bubble interactions in both biological systems, and industrial processes such as froth flotation separation of hydrophobic particles[1]. In most systems under normal atmospheric conditions, the nucleation of surface nanobubbles can hardly be avoided, resulting in a large range attraction force with a span of up to several hundred nanometres as measured by the conventional AFM (Atomic Force Microscopy) technique using the AFM colloid probes. In this conventional technique, the solid particle on the probe was first brought into contact with the solid substrate to establish the "zero" inter-surface separation distance and then cyclically separated from the contact and brought to the contact for a few times to allow an averaging of the actual data for the force curve which is expected to be statistically representative. This cyclical measurement of forces between hydrophobic surfaces is linked to the mechanical cavitation process, producing nanobubble bridges between the hydrophobic surfaces which have generated the key controversy over the long-ranged hydrophobic forces. The nature of these long-ranged forces is essentially capillary associated with the formation of a gas bridge between the surfaces (which can be eliminated as achieved in this paper).

Several mechanisms have been proposed to explain the origin of interaction between hydrophobic surfaces. Some of the most important existing theories include; the entropic origin originating from the configurational rearrangement of the vicinal water molecules between the hydrophobic surfaces[2-4], cavitation or separation induced phase transition[5-8], fluctuation correlation mechanisms, whereby confinement induces large density fluctuations that may result in anomalous hydrodynamic pressure[9], aqueous charge[10-11], or dipole correlations[12-13], Anomalous polarization of vicinal water molecules[14-15], and bridging of submicron bubbles also referred to the nanobubble bridging capillary force[16-17].

The proposed theories have been discussed by many researchers, but no consensus has been reached to date. Meyer et al.[18] compared the hydrophobic interactions between a symmetric system and an asymmetric system. The hydrophobic interactive forces were measured between two hydrophobic surfaces in the symmetric system, and between a hydrophobic and hydrophilic surface in an asymmetric system. The measured forces in both systems were found to be attractive and long-range, stronger than van der Waals. They reported the long-range attractive force can be explained by an electrostatic origin due to the alignment of oppositely charged surfaces in aqueous solutions, however, the attraction at the short-range, referred to as "truly hydrophobic" could not be explained. Tabor et al.[19] reviewed the application of common force measurement methods used in analyzing hydrophobic interactions. They reported that different measurement methods have evolved to allow the distinguishment of a true hydrophobic interaction from other interactions that can cause strong attractions. They highlighted that the true hydrophobic interaction at short range can be explained by the orientation of water molecules at hydrophobic surfaces but only at a very short range with a decay length of 3 Å. They discussed various origins can explain the interactions at large range such as nanobubbles, charge rearrangement correlations, and Hofmeister-type specific ion effects.

The long-range interaction between hydrophobic surfaces can be complicated by several factors such as contaminations, measurement methods, and other experimental conditions. Furthermore, other mechanisms, that are not directly associated with the short-range hydrophobic interaction, such as nanobubble bridging capillary force or cavitation can create uncertainty in studying the mechanism of interactions between hydrophobic surfaces. Therefore, researchers have attempted to minimize these uncertainties in experiments to probe the short-range hydrophobic interactions more accurately. Meyer et al.[20] studied the effect of dissolved gas removal on the attractive forces between hydrophobic surfaces. They discussed

the presence of two distinct long-range and short-range forces over the distance of 1000 Å down to contact between hydrophobic surfaces. No evidence of pre-existing surface nanobubbles was reported to account for the long-range attraction in this work. It was suggested the data were more consistent with cavitation and electrostatic origin mechanisms. The long-range attraction disappeared after the removal of the dissolved gases, however, the short-range attractive force still remained, which indicated the presence of two different mechanisms to account for this behavior. Ishida et al.[21] studied the interaction forces between hydrophobic surfaces in degassed aqueous solutions. They reported the presence of a short-range attractive force between the surfaces in the absence of bridging bubbles, that was stronger than the van der Waals attraction. The range of this force was estimated to be approximately 10-25 nm. The authors discussed this force to have a true hydrophobic origin which was affected by the surface hydrophobicity and was independent of bridging nanobubbles effect. The change in solution temperature and ionic strength showed a minimum effect on the attractive force, while the change in surface hydrophobicity changed the range and magnitude of the force considerably. To explain the origin of this force, Ishida et al.[21] discussed the possibility of the mechanism that involves dissolved gasses that reduce the density of water molecules around the surface and molecular vibration of solutions which can result in attractive force near the hydrophobic surface. The effect of salt on gas solubility in the bubble system has also been studied[22-23], however, the question about the origin of a distinctive short-range attractive force between hydrophobic surfaces remains open. Recent results suggest that thorough removal of dissolved gas results in surface interactions being in close agreement with the classic van der Waals model[24]. Indirectly, these findings propose that the origin of additional attractive force between hydrophobic surfaces should lie with the dissolved gas. In our previous study, it was shown that saturating aqueous salt solutions with gas results in an increased range of attractive forces even in the absence of nanobubble bridges[25]. It is, however, very challenging to precisely

control gas concentration by degassing or supersaturating, as it takes the system outside of thermodynamic equilibrium. Under such dynamic conditions, the measured forces may be strongly implicated by non-equilibrium gas concentration gradients associated with the non-zero mass transfer between the surface layer, bulk solution, and atmosphere. This uncertainty of controlling different constant levels of gas solubility in water by degassing in the force measurements using AFM can be amplified by the experimental practicalities which usually require a finite time for setting up, fine-tuning, and thermal equilibrium. Therefore, it is desired to avoid the degassing technique and to replace it by equilibrium control of gas solubility for the experiments.

To control the desired gas solubility in the aqueous solution for a long time and at equilibrium, in this paper, we have used salt solutions that are known to contain different concentrations of dissolved gases at equilibrium as a function of salt type and salt concentration. This work aims to examine the role of the dissolved gas on the attractive forces between hydrophobic surfaces by controlling the gas solubility using concentrated aqueous solutions of several 1:1 salts. The approach enables one to single out the effect of the dissolved gas and disentangle it from possible contributions from surface adsorption of ions.

2. Materials and Method

2.1 Materials

Silicon wafer surfaces (Silicon Valley Microelectronics, USA) and silica spheres of 20 μm in diameter (Fuso Chemicals Co. Ltd., Japan) were used as test surfaces. Glassware was cleaned using potassium hydroxide, ethanol, and water (1:8:1 ratio by weight) solutions with 15 min soaking and washing with pure (deionized, DI) water. AR grade ethanol was obtained from Crown Scientific (Australia). NH_4OH (AR grade) was purchased from Lab Services (Australia) and H_2O_2 (GR grade) from Merck. Sodium chloride (99.5%), Potassium Chloride,

Caesium Chloride, and Lithium Chloride were obtained from Sigma-Aldrich (Australia). The salts were baked for 6 hours before preparing salt solutions to avoid the possibility of contamination. DI water was freshly purified using a setup consisting of a reverse osmosis RIO's unit and an Ultrapure Academic Milli-Q system (Millipore, USA).

2.2 Surface hydrophobization

Esterification[26] with 1-octanol (Merck, Australia) was used to produce stable hydrophobic surfaces. The surfaces were first cleaned using acetone, ethanol, and water in an ultrasonic bath then soaked for 15 min in $5H_2O$:$1NH_4OH$:$1H_2O_2$ solution (RCA-SC1) at 75°C and rinsed with copious amounts of water, and dried under nitrogen gas stream[27]. The cleaned silica substrates were then immersed in boiling 1-octanol solution for 4h under reflux, rendering it hydrophobic. The silica particles were cleaned in the RCA-SC1 solution, washed with copious amounts of water, and dried in a desiccator, followed by esterification in 1-octanol for 4h, washed with acetone, and dried in a laminar flow cabinet. The advancing and receding water contact angles of hydrophobized surfaces, as measured by the sessile drop method using a PAT-1 pendant drop tensiometer system (SInterface Technologies, Germany), were 85° and 60°, respectively.

2.3 Equilibrium control of gas solubility in aqueous solutions

Figure 1 shows the equilibrium solubility of dissolved oxygen as a function of salt concentration for NaCl, LiCl, KCl, and CsCl aqueous solutions. As can be seen, the gas solubility is decreased with increasing the salt concentration. Different sets of salt concentrations can be chosen to provide a similar gas solubility. Likewise, each of the salts with the same concentration can give different four concentrations of dissolved gases. Here, we have selected four sets of salt concentrations as shown in Figure 1 to cover the whole range of dissolved oxygen and nitrogen of ambient clean air. The salt solutions were prepared by

dissolving the required amount of baked salts, equilibrated at room temperature (about 22 ^{o}C) for many days, and aerated using the nitrogen gas (purity 99.99 %) overnight before use. Dissolved oxygen (DO) was measured using a WTW Multi 3410 DO meter with WTW FDO 925® probe, which had been calibrated (calibration relative slope: 0.98 and FDO check: 99.3%). Incorporated into the WTW Multi 3410 meter is digital processing and data transfer, or stability control function, which allows the measurements to be very precise.

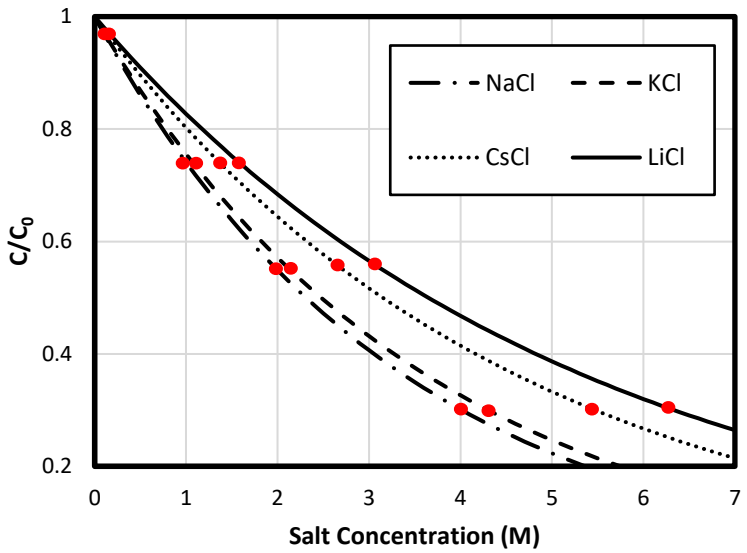

Figure 1. Experimental results for solubility of oxygen in salt solutions vs salt concentration[28]. C and C_o describe the concentration of dissolved oxygen in the salt solutions and DI water, respectively. Circles show the different salt concentrations with similar gas solubility, which were selected for the four sets of experiments.

2.4 Force measurements

Force measurements and AFM imaging were performed using an MFP-3D Asylum AFM (Asylum Research, USA). Force measurements were carried out using the colloidal probe technique[29-30] to determine the interaction forces between the hydrophobized silica particle and the hydrophobized silicon wafer substrates. Triangular cantilevers (BudgetSensors, Bulgaria)

with a nominal spring constant of 40 N/m were used. The actual spring constant was determined by the thermal method. The cantilevers were cleaned with piranha acid treatment, washed with DI water before use. AFM imaging was performed in liquid AC (tapping) mode.

To prevent the effect of mechanical cavitation by cyclical contacting and separating of hydrophobic surfaces and to capture the "short-range" attraction between hydrophobic surfaces in the absence the nanobubble bridges, we used the first contact approach force measurement method, in which we recorded and considered the first particle-substrate contact force curve.

2.5 Force analysis using the dense gas layer and multilayer dispersion theories

The measured force, *F*, **was** analyzed using **the sum of** the multilayer dispersion (**van der Waals**, **vdW) and electrostatic double-layer (edl) forces as** per the DLVO theory as **follows:** $F = -AR_p / \left(6h^2\right) + F_{edl}$, where R_p is the particle radius and *h* is the separation distance (i.e., the shortest thickness of the intervening liquid film between the surfaces). F_{edl} as a function of *h* was numerically calculated from the numerical solution of the Poisson-Boltzmann equations (PBE). The details of the calculations are described in the supplementary information. Likewise, the van der Waals force as described by the first term on the right-hand side of the equation shown above was numerically calculated using the multilayer dispersion theory[31]. The Hamaker function, *A*, is not a constant but depends on separation distance due to the effect of the finite speed of light (known as the retardation or Casimir-Folder effect[32]). As described in the SI, here we consider a 7-layer system which consists of the water layer at the center, two dense gas layers (DGLs), two simple surfactant layers of esterification, and two silicon wafer materials. Each of the two DGLs is sandwiched between the solid surface hydrophobized by esterification using ethanol and the aqueous phase[33-34]. A brief discussion about DGLs is given in the next section.

3 Results and discussion

In force-distance measurements, the salt concentrations were chosen to have matching gas solubility as described in the experimental section. Specifically, the four salt concentrations used for the experiments are shown by red circles in Figure 1. The results of force measurements in the aqueous solutions at four levels of gas solubility are shown in Figure 2. For each of the salts, decreasing the content of dissolved gases results in a decrease in the magnitude of the attractive force as well as shortening of its range. Still, the range of the attractive force is considerably larger than that expected for vdW attraction between octanol-esterified silicon wafer surfaces in the solutions. The results of AFM measurements for different salt types and concentrations are summarised in Table 1. We note that the attractive force in different salts with the same concentration is different, which excludes the possibility that the observed changes are dominated by non-linear polarizability effects observed in the concentrated 1:1 salt solutions. In such a case, one would expect the force to be the strong function of the salt concentration.

Furthermore, the concentration of dissolved oxygen for the different salt solutions and concentrations, used in the AFM measurements, were measured using the dissolved oxygen probe. The experimental measurements of dissolved oxygen show a decrease in the gas content for the different salt solutions and concentrations, as presented in Table 1. It was observed that the attraction range between hydrophobic surfaces is decreased with increasing the salt concentration in the absence of the nanobubble bridges. This suggests that the dissolved gases, the content of which decreases with the increase in salt concentration, affect the attraction between hydrophobic surfaces.

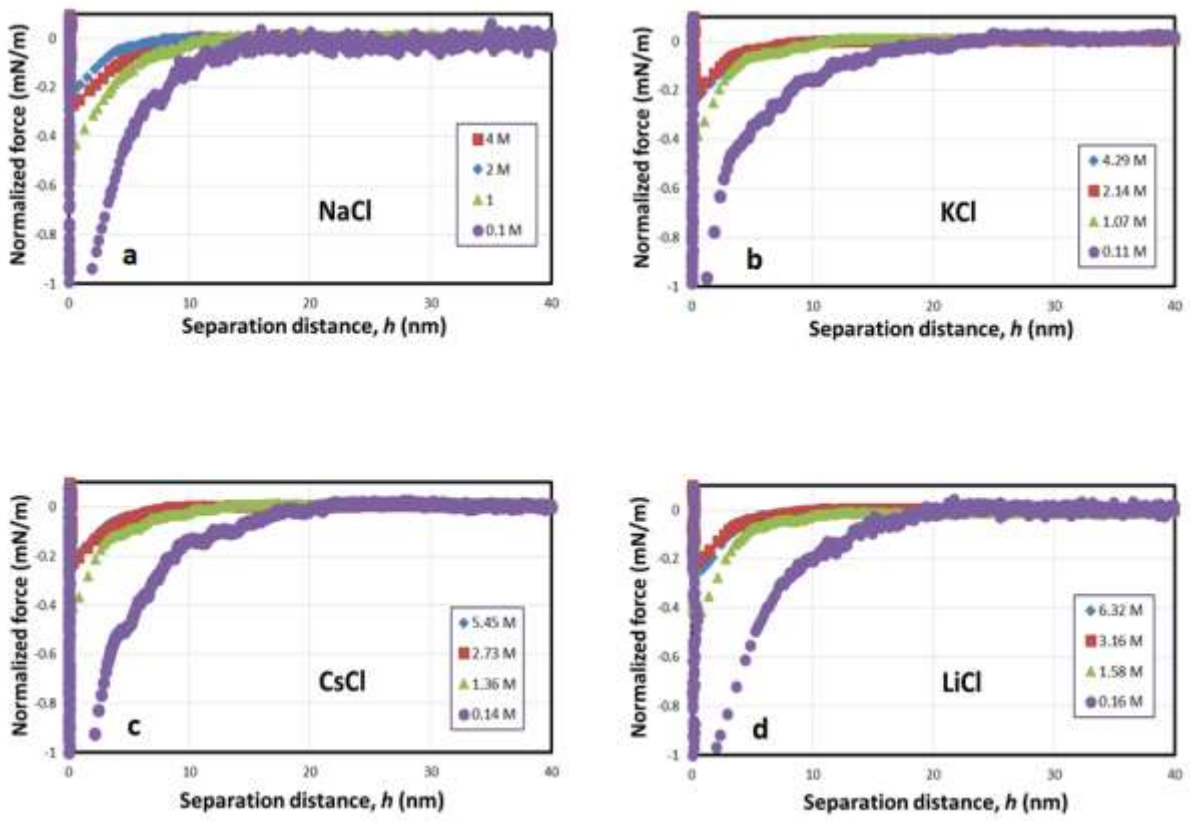

Figure 2. Comparison of the force curves at different concentrations of different aqueous solutions of NaCl, KCl, CsCl, and LiCl as chosen per Figure 1. The force is normalized by dividing the measured force by the particle radius.

Table 1. Summary and results of the force measurements and measured dissolved oxygen.

Salt types and concentrations	C/C_0	Measured dissolved oxygen (μM)	Calculated DGL thickness (nm)	Measured attraction range (nm)
0.1 M NaCl	0.970446	256.3±0.5	4.88±0.20	15-19
0.11 M KCl		244.7±0.7	4.84±0.081	
0.14 CsCl		248.2±0.6	5.1±0.08	
0.16 LiCl		261.6±0.5	5.14±0.16	
1 M NaCl	0.740818	213.4±0.5	2.38±0.05	11-14
1.07 M KCl		208.7±0.5	2.28±0.04	
1.36 M CsCl		201.1±0.7	2.34±0.04	

1.58 LiCl		205.4±0.8	2.38±0.04	
2 M NaCl	0.548812	178.1±0.6	1.4±0.06	9-11
2.14 M KCl		185.8±0.9	1.25±0.05	
2.73 M CsCl		171.2±0.7	1.3±0.1	
3.16 M LiCl		167.4±0.6	1.3±0.06	
4M NaCl	0.301194	131.3±0.6	1.24±0.07	8-10
4.29 M KCl		116.8±0.9	1.4±0.08	
5.45 M CsCl		128.1±0.8	1.3±0.03	
6.32 M LiCl		121.8±0.6	1.4±0.04	

Dissolved gases can preferentially accumulate and enrich at the hydrophobic surfaces in water as interfacial nanobubbles and nanopancakes which are nowadays known as gaseous domains on immersed hydrophobic solid surfaces in water and can survive for days[35]. These gas domains were first discussed in the context of strong attraction between hydrophobic surfaces in aqueous solutions as measured by the surface force apparatus, based on the discontinuities of the Newton rings (the fringes used to measure separation distances spectroscopically) by spontaneous cavitation occurring at contacting hydrophobic surfaces[6, 18]. The interfacial nanobubbles were then connected with the stepwise features in measured force curves, now known as the nanobubble bridging capillary force[36], and confirmed by AFM imaging on a variety of hydrophobic surfaces and many other non-AFM techniques[37]. In this paper, we have eliminated the nanobubble bridging force experimentally and have considered the effect of interfacial gas enrichment (IGE) of dissolved gases at the hydrophobic surface on the measured force. The IGE covering the entire area of the hydrophobic solid-water interface is responsible for the unexpected stability of interfacial gaseous domains[38]. Also, the molecular attraction between the gas molecules of IGE and the hydrophobic surface forms a dense gas layer (DGL) adjacent to the hydrophobic surface, providing the molecular stability of the interfacial gaseous domains[33]. The DGL has been included in analyzing the dispersion force as described in Section 2.5. Figure 3 shows the comparison of the measured force curve in 4M

NaCl solution with the theory with the inclusion of the 7-layer (silica-octanol-DGL-aqueous solution-DGL-octanol-silica) dispersion force model. The model agrees well with the measurements, which supports the possibility of a gas layer formation on the hydrophobic surfaces, extending the surface interactions to a larger range and magnitude

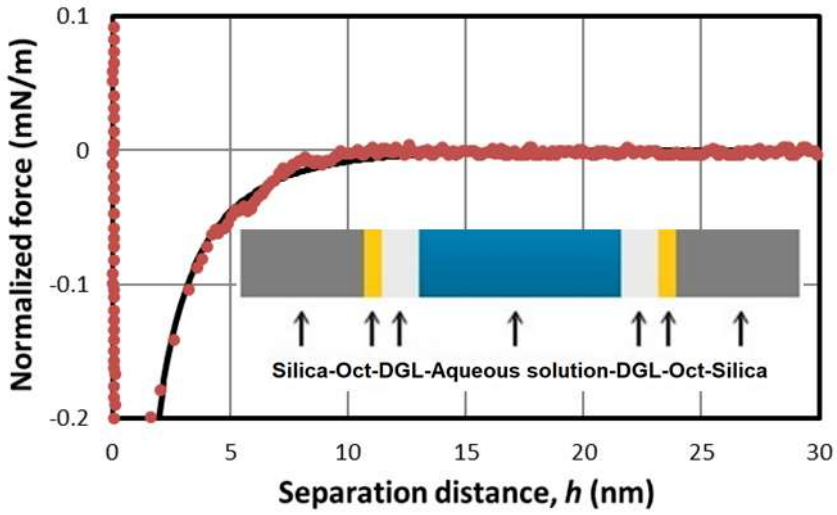

Figure 3. Measured force (red circles) in 4 M NaCl solution versus theoretical force (black line) with the 7-layer dispersion model as described in Section 2.5. The forces are normalized by dividing by the particle radius. The DGL thickness is 1.2 nm.

Figure 4 shows the predicted DGL thickness versus salt concentration as calculated by comparing the force model with the measured force curves for different salt solutions. It was observed that the predicted thickness of DGLs was thicker for lower salt concentrations, while a smaller thickness of DGLs was observed for higher salt concentrations. We predict that in higher salt concentrations, with lower gas solubility, the formation of a gas layer on the surface is more limited, and hence a thinner gas layer is formed. In the solutions with lower salt concentrations and higher gas solubility, the possibility of the formation of a larger gas layer is higher. Comparison of the predicted DGL thickness for different salt types at salt concentrations with similarly dissolved gas solubilities shows that at salt concentrations with

similar gas solubilities, a similar length of gas layers has been observed for different salts, as shown in Figure 4. These results agree with the hypothesis that the dissolved gas content, affected by the salt concentration, is a crucial factor for controlling the attractive force between the hydrophobic surfaces, in the absence of nanobubble bridging capillary force. They are also supported by the recent literature which has pointed to the critical role of dissolved gases in aqueous thin films affecting dispersion forces in a wide range of important phenomena[39-40]. However, a few issues remain to be solved, including the effect of salts on the water dielectric function (or polarizability) that affects the calculation of dispersion forces as shown in the SI, where the salt effect is only accounted for by the zero-frequency term.

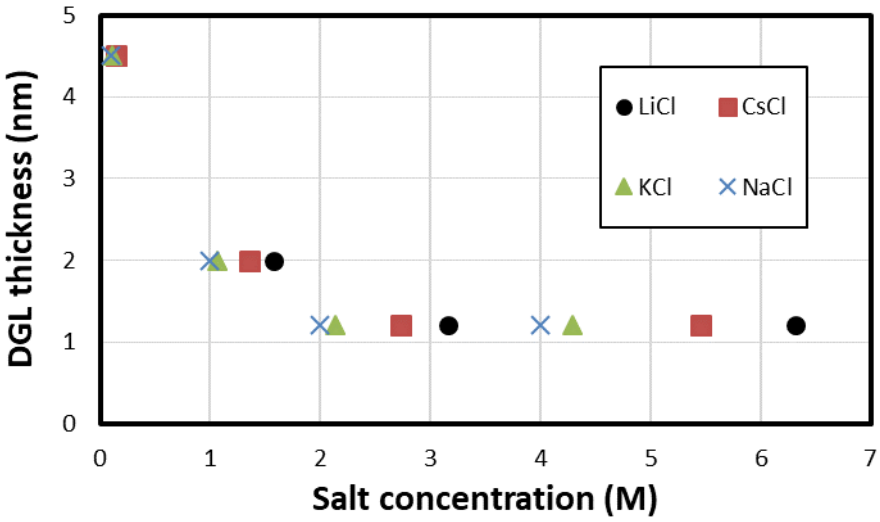

Figure 4. Predicted DGL thickness versus salt type and concentrations. The salt concentrations used for measurements with similar gas solubilities as shown in Figure 1.

4. Conclusions

We have successfully studied the short-range attractive force between hydrophobized silica surfaces in aqueous solutions of well-controlled solubility of dissolved gases. We have employed the first contact approach of the AFM colloid probe force measurements and, therefore, have eliminated the nanobubble bridge capillary force. Choosing four sets of

different salts (NaCl, KCl, CsCl, and LiCl) and different concentrations have provided four consistent levels of dissolved gas solubility, uniformly spanning between the gas solubilities in DI water and salt-saturated solutions. We have observed that the range and magnitude of the short-range force between the hydrophobic surfaces decreased with decreasing concentration of dissolved gases in the aqueous solutions. However, this dependency did not scale with salt concentration. Instead, we have found that across all four salt types the force scaled with dissolved gas concentration, so that the measured attraction between hydrophobic surfaces in solutions with different salt concentrations but matching the gas solubility was very similar. When analyzing the experimental results, we have applied a multilayer (silica-octanol-DGL-aqueous solution-DGL-octanol-silica) dispersion force model. The water dielectric function was numerically calculated using the latest experimental data for the real and imaginary parts of the complex dielectric function of liquid water (up to the frequency of 100 eV). A good agreement with the experimental results was achieved by evoking IGE concept that results in the formation of DGL at the hydrophobic surface. It is corroborated that the DGL thickness decreases with decreasing gas solubility up to a length of ca. 14 Å beyond which it remains constant. These findings agree with the hypothesis that dissolved gases control the attractive force between hydrophobic surfaces.

AUTHOR INFORMATION

Corresponding Author

Correspondence should be addressed to mehdi.azadi@uq.edu.au (Mehdi Azadi) and anh.nguyen@eng.uq.edu.au (Anh V. Nguyen).

Author Contributions

The manuscript was written through the contributions of all authors. All authors have approved the final version of the manuscript.

Note

The authors declare no competing financial interest.

ACKNOWLEDGMENT

We gratefully acknowledge financial support from the Australian Research Council (grant DP0985079), and the International Postgraduate Research Scholarship (IPRS) and UQ Centennial Scholarship (UQCent) awarded to M.A. G.Y. acknowledges support from the ARC Centre of Excellence in Plant Cell Walls research fellowship.

References

1. Nguyen, A. V.; Schulze, H. J., *Colloidal science of flotation*. Marcel Dekker: New York, 2004; p 840.
2. Israelachvili, J. N.; Pashley, R. M., Measurement of the hydrophobic interaction between two hydrophobic surfaces in aqueous electrolyte solutions. *Journal of Colloid and Interface Science* **1984,** *98* (2), 500-514.
3. Claesson, P. M.; Blom, C. E.; Herder, P. C.; Ninham, B. W., Interactions between water—stable hydrophobic Langmuir—Blodgett monolayers on mica. *Journal of Colloid and Interface Science* **1986,** *114* (1), 234-242.
4. Eriksson, J. C.; Ljunggren, S.; Claesson, P. M., A phenomenological theory of long-range hydrophobic attraction forces based on a square-gradient variational approach. *Journal of the Chemical Society, Faraday Transactions 2: Molecular and Chemical Physics* **1989,** *85* (3), 163-176.
5. Yaminsky, V. V.; Yushchenko, V. S.; Amelina, E. A.; Shchukin, E. D., Cavity formation due to a contact between particles in a nonwetting liquid. *Journal of Colloid and Interface Science* **1983,** *96* (2), 301-306.
6. Christenson, H. K.; Claesson, P. M., Cavitation and the interaction between macroscopic hydrophobic surfaces. *Science* **1988,** *239* (4838), 390-392.
7. Yaminsky, V. V.; Ninham, B. W., Remarks on the Limitation of the Range of the Hydrophobic Force. *Langmuir* **1996,** *12* (20), 4969-4970.
8. Wood, J.; Sharma, R., How Long Is the Long-Range Hydrophobic Attraction? *Langmuir* **1995,** *11* (12), 4797-4802.
9. Ruckenstein, E.; Churaev, N., A possible hydrodynamic origin of the forces of hydrophobic attraction. *Journal of Colloid and Interface Science* **1991,** *147* (2), 535-538.
10. Podgornik, R., Electrostatic correlation forces between surfaces with surface specific ionic interactions. *The Journal of Chemical Physics* **1989,** *91* (9), 5840-5849.
11. Podgornik, R.; Parsegian, V. A., An electrostatic-surface stability interpretation of the "hydrophobic" force inferred to occur between mica plates in solutions of soluble surfactants. *Chemical Physics* **1991,** *154* (3), 477-483.
12. Attard, P., Long-range attraction between hydrophobic surfaces. *Journal of Physical Chemistry* **1989,** *93* (17), 6441-6444.
13. Rabinovich, Y. I.; Guzonas, D. A.; Yoon, R. H., Role of chain order in the long-range attractive force between hydrophobic surfaces. *Langmuir* **1993,** *9* (5), 1168-1170.
14. Rabinovich, Y. I.; Deryagin, B. V., DIRECT MEASUREMENT OF FORCES OF ATTRACTION OF HYDROPHOBIZED QUARTZ FIBERS IN AQUEOUS KCl SOLUTIONS. *Colloid journal of the USSR* **1987,** *49* (4), 598-602.
15. Rabinovich, Y. I.; Derjaguin, B. V., Interaction of hydrophobized filaments in aqueous electrolyte solutions. *Colloids and Surfaces* **1988,** *30* (3-4), 243-251.

16. Parker, J. L.; Claesson, P. M.; Attard, P., Bubbles, cavities, and the long-ranged attraction between hydrophobic surfaces. *Journal of Physical Chemistry* **1994,** *98* (34), 8468-8480.
17. Attard, P., Bridging Bubbles between Hydrophobic Surfaces. *Langmuir* **1996,** *12* (6), 1693-1695.
18. Meyer, E. E.; Lin, Q.; Hassenkam, T.; Oroudjev, E.; Israelachvili, J. N., Origin of the long-range attraction between surfactant-coated surfaces. *Proceedings of the National Academy of Sciences of the United States of America* **2005,** *102* (19), 6839-6842.
19. Tabor, R. F.; Grieser, F.; Dagastine, R. R.; Chan, D. Y. C., The hydrophobic force: Measurements and methods. *Physical Chemistry Chemical Physics* **2014,** *16* (34), 18065-18075.
20. Meyer, E. E.; Lin, Q.; Israelachvili, J. N., Effects of dissolved gas on the hydrophobic attraction between surfactant-coated surfaces. *Langmuir* **2005,** *21* (1), 256-259.
21. Ishida, N.; Kusaka, Y.; Ushijima, H., Hydrophobic attraction between silanated silica surfaces in the absence of bridging bubbles. *Langmuir* **2012,** *28* (39), 13952-13959.
22. Craig, V. S. J.; Ninham, B. W.; Pashley, R. M., Effect of electrolytes on bubble coalescence. *Nature* **1993,** *364* (6435), 317-319.
23. Browne, C.; Tabor, R. F.; Chan, D. Y. C.; Dagastine, R. R.; Ashokkumar, M.; Grieser, F., Bubble coalescence during acoustic cavitation in aqueous electrolyte solutions. *Langmuir* **2011,** *27* (19), 12025-12032.
24. Mastropietro, D. J.; Ducker, W. A., Forces between hydrophobic solids in concentrated aqueous salt solution. *Physical Review Letters* **2012,** *108* (10).
25. Azadi, M.; Nguyen, A. V.; Yakubov, G. E., Attractive forces between hydrophobic solid surfaces measured by AFM on the first approach in salt solutions and in the presence of dissolved gases. *Langmuir* **2015,** *31* (6), 1941-1949.
26. Biggs, S.; Grieser, F., Atomic Force Microscopy Imaging of Thin Films Formed by Hydrophobing Reagents. *Journal of Colloid and Interface Science* **1994,** *165* (2), 425-430.
27. Hampton, M. A.; Donose, B. C.; Taran, E.; Nguyen, A. V., Effect of nanobubbles on friction forces between hydrophobic surfaces in water. *Journal of Colloid and Interface Science* **2009,** *329* (1), 202-207.
28. Weissenborn, P. K.; Pugh, R. J., Surface Tension of Aqueous Solutions of Electrolytes: Relationship with Ion Hydration, Oxygen Solubility, and Bubble Coalescence. *Journal of Colloid and Interface Science* **1996,** *184* (2), 550-563.
29. Ducker, W. A.; Senden, T. J.; Pashley, R. M., Direct measurement of colloidal forces using an atomic force microscope. *Nature* **1991,** *353* (6341), 239-241.
30. Butt, H.-J., Measuring electrostatic, van der Waals, and hydration forces in electrolyte solutions with an atomic force microscope. *Biophysical Journal* **1991,** *60* (6), 1438-1444.
31. Parsegian, V., *Van der Waals forces*. Cambridge Uinversity Press: Cambridge 2006.
32. Mahanty, J. H.; Ninham, B. W., *Dispersion Forces*. Academic Press: London, 1977; p 236.
33. Peng, H.; Birkett, G. R.; Nguyen, A. V., Origin of Interfacial Nanoscopic Gaseous Domains and Formation of Dense Gas Layer at Hydrophobic Solid-Water Interface. *Langmuir* **2013,** *29* (49), 15266-15274.
34. Doshi, D. A.; Watkins, E. B.; Israelachvili, J. N.; Majewski, J., Reduced water density at hydrophobic surfaces: Effect of dissolved gases. *Proc. Natl. Acad. Sci. U. S. A.* **2005,** *102* (27), 9458-9462.
35. Ball, P., Nanobubbles are not a Superficial Matter. *ChemPhysChem* **2012,** *13* (8), 2173-2177.
36. Hampton, M. A.; Nguyen, A. V., Nanobubbles and the nanobubble bridging capillary force. *Adv. Colloid Interface Sci.* **2010,** *154* (1-2), 30-55.
37. Lohse, D.; Zhang, X., Surface nanobubbles and nanodroplets. *Reviews of Modern Physics* **2015,** *87* (3), 981-1035.
38. Peng, H.; Birkett, G. R.; Nguyen, A. V., Progress on the Surface Nanobubble Story: What is in the bubble? Why does it exist? *Adv. Colloid Interface Sci.* **2015,** *222*, 573-580.

39. Fiedler, J.; Parsons, D. F.; Burger, F. A.; Thiyam, P.; Walter, M.; Brevik, I.; Persson, C.; Buhmann, S. Y.; Bostroem, M., Impact of effective polarizability models on the near-field interaction of dissolved greenhouse gases at ice and air interfaces. *Phys. Chem. Chem. Phys.* **2019,** *21* (38), 21296-21304.
40. Bostrom, M.; Corkery, R. W.; Lima, E. R. A.; Malyi, O. I.; Buhmann, S. Y.; Persson, C.; Brevik, I.; Parsons, D. F.; Fiedler, J., Dispersion Forces Stabilize Ice Coatings at Certain Gas Hydrate Interfaces That Prevent Water Wetting. *ACS Earth Space Chem.* **2019,** *3* (6), 1014-1022.

Supplementary information

Numerical calculation of model forces

For multilayer silica-octanol-DGL-aqueous solution-DGL-octanol-silica system, the Hamaker function can be calculated applying the multilayer dispersion force theory[1] which gives:

$$A = -\frac{3k_BT}{2}\sum_{n=0}^{\infty}{}' \int_{x_n}^{\infty} x \ln\left[\left\{1-\bar{\Delta}_{mL}(i\omega_n)\bar{\Delta}_{mR}(i\omega_n)e^{-x}\right\}\left\{1-\Delta_{mL}(i\omega_n)\Delta_{mR}(i\omega_n)e^{-x}\right\}\right] \mathrm{d}x \qquad (1)$$

where x is the integration dummy, k_B is the Boltzmann constant and T is the absolute temperature. The prime against the summation in n indicates that the zero-frequency (n = 0) term is divided by 2. The Matsubara (sampling, discrete equally spaced) frequencies are described by $\omega_n = 2n\pi k_BT/\hbar$ where $\hbar$ is the Planck constant (divided by 2π), while $i\omega_n$ are the imaginary frequencies. $x_n = 2h\omega_n\sqrt{\varepsilon_m(i\omega_n)}/c$, where c is the speed of light and $\varepsilon_m(i\omega_n)$ is the dielectric function of the liquid medium (the aqueous salt solution) between the two multilayered structures. Δ_{mL} and Δ_{mR} describe the diamagnetic reflection coefficients of a photon passing across the multilayered structure between the liquid medium and the semi-infinite substrate (L) on the left, and the multilayered structure between the medium and the semi-infinite substrate (R) on the right, respectively. If the left multilayer consists of N layers of thickness h_i with $i = 1,2,...,N$ (the 1st layer is next to the substrate and the last layer N is next to the liquid medium), we have

$$\Delta_{mL} = \frac{\Delta_{mN} + \Delta_{NL}(h_1,h_2,...,h_{N-1})\exp\left[-xh_Ns_N/(ph)\right]}{1+\Delta_{mN}\Delta_{NL}(h_1,h_2,...,h_{N-1})\exp\left[-xh_Ns_N/(ph)\right]} \qquad (2)$$

where the diamagnetic reflection coefficient for the multilayered structure of the sequentially reduced number of layers can be calculated using a recursion equation as follows:

$$\Delta_{jL} = \frac{\Delta_{j(j-1)} + \Delta_{(j-1)L}(h_1,h_2,...,h_{j-2})\exp\left[-xh_{j-1}s_{j-1}/(ph)\right]}{1+\Delta_{j(j-1)}\Delta_{(j-1)L}(h_1,h_2,...,h_{j-2})\exp\left[-xh_{j-1}s_{j-1}/(ph)\right]} \text{ for } j = N, N-1,...,2 \qquad (3)$$

The zeroth layer is the substrate *L* on the left. For nonmagnetic materials considered in this paper, the diamagnetic reflection coefficient of a photon passing across a single interface between two materials "*j*" and "*k*" which is required in Eqs. (2) and (3) is calculated as follows:

$$\Delta_{jk}(i\omega) = \frac{s_j - s_k}{s_j + s_k} \tag{4}$$

The retardation coefficients in Eq. (4) are defined by

$$s_j(i\omega) = \sqrt{p^2 - 1 + \varepsilon_j(i\omega)/\varepsilon_m(i\omega)} \tag{5}$$

where $\varepsilon_j(i\omega)$ is the dielectric function of the material "*j*". The parameter *p* is defined by

$$p = \frac{xc}{2\omega h\sqrt{\varepsilon_m(i\omega)}} \tag{6}$$

For the multilayered structure on the right, Δ_{mR} can be calculated using similar equations.

In Eq. (1), $\bar{\Delta}_{mL}$ and $\bar{\Delta}_{mR}$ describe the dielectric reflection coefficients of a photon passing across the multilayered structures on the left and the right sides of the medium, respectively. They can be calculated using Eqs. (2) and (3) with the symbol "Δ" being replaced by $\bar{\Delta}$, and the dielectric reflection coefficient of a photon passing across a single interface being calculated as follows:

$$\bar{\Delta}_{jk}(i\omega) = \frac{s_j\varepsilon_j - s_k\varepsilon_k}{s_j\varepsilon_j + s_k\varepsilon_k} \tag{7}$$

We also accounted for the effect of screening of the vdW interactions by salts by adjusting the zero-frequency term, A_0, as follows:

$$A_0(\kappa) = A_0(0)(1 + 2\kappa h)\exp(-2\kappa h) \tag{8}$$

The Debye constant in Eq. (8) is defined by:

$$\kappa = \sqrt{2000 N_A e^2 I / \left(\varepsilon \varepsilon_0 k_B T\right)} \tag{8}$$

where I is the solution ionic strength in mol/L (M), N_A is the Avogadro number, ε is the permittivity of the vacuum, $\varepsilon_0 = 78$ is the dielectric constant of water, e is the charge on the electron.

The required spectrum of dielectric function of liquid water was calculated by numerically integrating the Kramers-Kronig equation using the latest experimental data for the real and imaginary parts of the complex dielctric function of liquid water (up to the frequency of 100 eV) [2], i.e., not using the data obtained by the oscillator model approximation. Spectral data for octanol could not be located so they were approximated using "Cauchy plots" [3] using absorption parameters for octane [4] (the alkane portion of octanol). The thickness of the octanol layer was assumed to be 1 nm. The dielectric functions for dense gas layers and air are assumed to be 1 in the calculation.

The numerical integration of Eq. (1) was best carried out using quadratures with high-degree polynomial fitting such as the Gauss-Laguerre formulas for the infinite interval[5]. The computational results reported here were obtained using the values of the zeros of the Laguerre polynomial and the respective weights of the 30th order Gauss-Laguerre quadrature. The computation of the outer summation included about 3000 or more terms for satisfactory convergence and accuracy (with a relative error smaller than 0.001% for the summation).

The edl force was calculated using the numerical solution of the Poisson-Boltzmann equations (PBE) together with the assumption of either constant surface potential or constant surface charge[5]. Specifically, PBE for two flat surfaces was first numerically solved employing the collocation method for a system of differential equations subject to nonlinear, two-point boundary conditions at the surfaces. Together with the boundary conditions, the discretized equations on a uniform 1D mesh form a system of nonlinear algebraic equations for the electrical potential between the two surfaces and its gradient (first derivative), which can be solved iteratively by linearization employing the linear equation solvers of Matlab. The approximate Debye-Hückel solution of PBE was used to initialize the numerical solution by the collocation method. After obtaining the electrical potential, ψ, between the flat surfaces and its gradient $d\psi / dx$, the edl disjoining pressure as a function of the separation between the surfaces was calculated using the Langmuir equation described by

$\Pi_{edl} = k_B T \sum n_i \left[\exp\left(-z_i \psi e / k_B T\right) - 1 \right] - \varepsilon\varepsilon_0 \left(d\psi / dx\right)^2 / 2$, where n_i the number concentration of the salt ions "*i*" with charge z_i and the summation is considered for all types of ions in solution. The Langmuir equation is valid at all points between the surfaces, but was conveniently evaluated using the potential and its gradient at one of the surfaces here. Knowing the disjoining pressure as a function of separation distance, the edl interaction force between the colloid probe and the flat surface was calculated by applying the Derjaguin approximation as follows:

$$F_{edl}(h) = 2\pi R_p \int_h^\infty \Pi(\eta)\, d\eta \tag{8}$$

The integration was carried out using the function Quad of MATLAB. In the integration, the pressure as a function of separation distance was approximated using the numerical values and the interpolation function of MATLAB. The integration limit at infinity was replaced by a finite distance (typically of $20/\kappa$) and the superposition solutions of PBE (for analytically evaluating the integral from the finite distance to infinity)[5].

References

1. Parsegian, V., *Van der Waals forces*. Cambridge Uinversity Press: Cambridge 2006.
2. Wang, J.; Nguyen, A. V., A review on data and predictions of water dielectric spectra for calculations of van der Waals surface forces. *Adv. Colloid Interface Sci.* **2017,** *250*, 54-63.
3. Hough, D. B.; White, L. R., The calculation of Hamaker constants from Lifshitz theory with applications to wetting phenomena. *Adv. Colloid Interface Sci.* **1980,** *14* (1), 3-41.
4. Israelachvili, J. N., *Intermolecular and Surface Forces*. Academic Press: London, 2005; p 291.
5. Nguyen, A. V.; Schulze, H. J., *Colloidal science of flotation*. Marcel Dekker: New York, 2004; p 840.